Molecular Design, Syntheses, and Physical Properties of Nonpolymeric Amorphous Dyes for Electron Transport

Katsuyuki Naito,* Masatoshi Sakurai, and Syun Egusa

Advanced Research Laboratory, Research and Development Center, Toshiba Corporation, 1 Komukai-Toshiba-cho, Saiwai-ku, Kawasaki 210, Japan

Received: October 18, 1996; In Final Form: January 3, 1997[⊗]

Relationships between electrical properties and molecular structures for various nonpolymeric amorphous dyes were investigated. Absorption maximum wavelengths (λ_{obs}) for amorphous films were found to be nearly equal to those for solution samples. When the parameters of the used PPP−CI MO method were modified so as to reproduce the λ_{obs} values, the calculated HOMO and LUMO energy levels corresponded with the reported ionization potential (I_p) and electron affinity (E_A) values. Electric carrier transport properties between dye films and metal electrodes (Au or Al) were found to be correlated with the HOMO and LUMO levels. For strong donor and acceptor dyes, impurity carrier effects were generally observed. For weak donor and acceptor dyes, carrier injection was difficult. Carrier injection phenomena without the influence of impurities were observed for moderate donor and acceptor dye films. Amorphous dyes with cyanovinyl substituents or oxadiazole rings were designed to allow reversible electron transport and were newly synthesized.

Introduction

A number of studies have recently been performed on amorphous (glass) thin films consisting of thermally stable nonpolymeric organic dye molecules as a result of their potential for use in optical and electrical application such as organic electroluminescent (EL) devices[1] and rewritable color recording media,[2] etc. Polycrystalline films prepared by conventional methods, such as physical vapor deposition (PVD), always have grain boundaries of various sizes. These cause serious structural defects and deep carrier traps. Therefore, the deposition of amorphous thin films seems to be a good alternative approach for the production of uniform thin films of functional dyes.

Many studies have been carried out on various types of glass containing organic materials.[3] However, nonpolymeric organic dye glasses have been considered to be thermally unstable. Efforts to synthesize amorphous dyes have been aimed at mainly dissolving them as much as possible in thermally stable amorphous polymers, not to improve their own thermal stability. In previous papers,[4,5] we have described the quantitative relationship between amorphous parameters such as glass transition temperature (T_g) and thermodynamic parameters related to phase transitions. The results have indicated that it is possible to make heat-resistive and stable nonpolymeric organic dye glasses from large, symmetric, rigid, and dense molecules. Furthermore, network dye molecules with multiple hydrogen-bonding sites showing a T_g value as high as 500 K have been synthesized.

The next step is the control of optical and/or electrical properties of organic dye glasses by appropriate molecular design. The properties of various dye moieties have already been reported by many researchers from the viewpoint of device performance, etc. Electric carrier injection from an electrode to an organic film, injected carrier transport in the film, and ejection to another organic film or another electrode are important properties for EL devices,[6] photocells, organic photoconductors, and other electronic devices. Relative to hole-transporting dyes, there are fewer good electron-transporting organic dyes. This has inhibited the development of devices using these dyes. Some amorphous dyes[1] and polymer materials[7] have been used as an electron transporting dye in organic EL devices,[1] but their electron transport capabilities including injection and ejection are not yet sufficient.

The present paper investigates the relationship between the molecular structures of various nonpolymeric organic dyes and their electrical properties using a PPP−CI quantum chemical calculation method.[8] In order to discuss the properties in the condensed states, it was necessary to determine the appropriate parameters for use in the semiempirical method. New amorphous dyes with a cyano group were designed using the PPP method, and they were synthesized.

Materials and Methods

Materials. Figure 1 shows the organic compounds discussed in this study. The CVB-S and OXD-S compounds were newly synthesized. CVB-1,2,3,4, OXD-7,8, DPNTCI, DCDPBAQ, TCPE, DNIBPC, and TBAQ were synthesized according to the pertinent literature.

The CVB-S compounds were synthesized in cooperation with Toyotama Koryo Co., Ltd. (Japan) through a condensation reaction between 1,3,5-triformylbenzene (TFB) (Sogo Pharmaceutical Co., Ltd., Japan) and α-cyanomethylene compounds (Tokyo Chemicals Industry Co., Ltd., Japan) in the presence of a base.

Synthesis of 1,3,5-Tris(2,2-dicyanoethenyl)benzene (CVB-S1). TFB (3.24 g, 20 mmol), malononitrile (5.9 g, 90 mmol), boron oxide (1.0 g), and ethanol (80 mL) were refluxed for 2 h. The ethanol was evaporated under a reduced pressure. The residue was extracted with acetonitrile (150 mL) and filtered. The acetonitrile was evaporated under a reduced pressure to give the crude product (1.5 g), which was recrystallized from a hexane/ethanol (1/1 v/v) solution. A total of 0.9 g of crystalline powder was obtained (15% yield). Mp: 270 °C. IR (KBr, cm^{-1}): 3100 (m), 3050 (s), 1950 (m), 2250 (s, CN), 1605 (vs, Ph), 1580 (s), 1460 (s), 1200 (vs), 960 (vs), 680 (vs), 620 (vs). H-NMR (DMSO-d_6, ppm): 8.79 (s, CH═, 1 H), 8.48 (s, Ph−H, 1 H). Anal. calcd. for $C_{18}H_6N_6$: C, 70.59; H, 1.97; N, 27.40. Found: C, 69.74; H, 2.00; N, 27.15. TLC(SiO_2, benzene/ethyl acetate = 95/5 v/v): R_f = 0.55 (single spot).

* Author to whom correspondence should be addressed.

[⊗] Abstract published in *Advance ACS Abstracts,* March 1, 1997.

S1089-5639(96)03233-1 CCC: $14.00

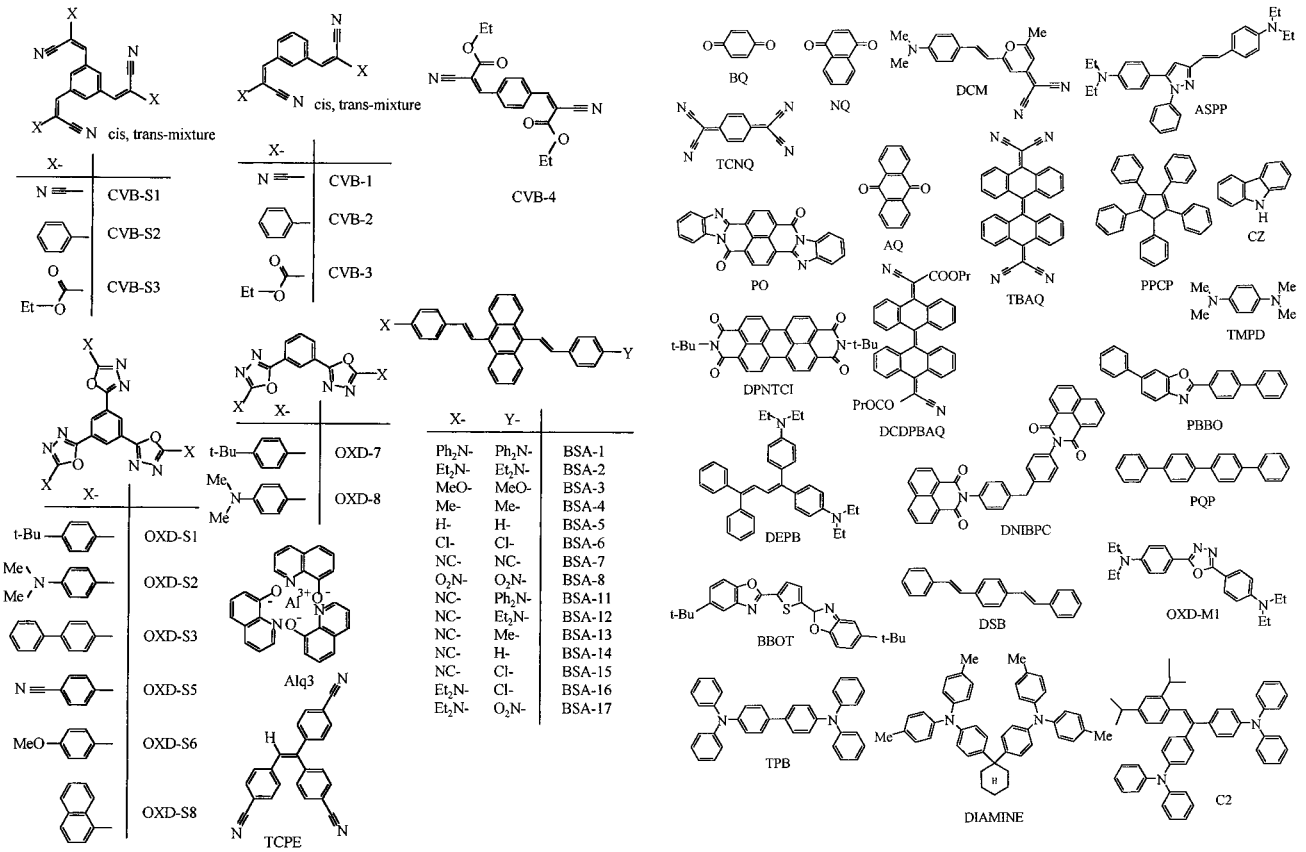

Figure 1. Molecular structures of organic dye compounds used in this study.

Synthesis of 1,3,5-Tris(2-cyano-2-phenylethenyl)benzene (CVB-S2). TFB (3.24 g, 20 mmol) and phenylacetonitrile (10.5 g, 90 mmol) were dissolved in 50 ml of ethanol. The mixture was cooled to 5 °C, and sodium ethoxide (2.0 g, 30 mmol) was added over a period of 30 min. The reaction mixture was stirred at room temperature for 2 h. The residue was extracted with toluene (100 mL) and washed with water. The toluene solution was dried over magnesium sulfate. The toluene was evaporated under a reduced pressure to give the crude product (12.79 g). The product was purified by column chromatography (SiO_2, toluene/ethyl acetate = 95/5 v/v). A total of 2.0 g of crystalline powder was obtained by crystallization from *n*-hexane (22% yield). Mp: 270 °C (broad). IR (KBr, cm^{-1}): 3060 (m, Ph), 3040 (m, Ph), 2240 (w, CN), 2220 (s, CN), 1600 (s, Ph), 1595-(sh), 1500(vs), 1455(vs), 905(s), 770(vs), 700(vs). H-NMR ($CDCl_3$, ppm): 8.3−7.0 (complex). Anal. calcd. for $C_{33}H_{21}N_3$: C, 86.25; H, 4.61; N, 9.14. Found: C, 85.57; H, 4.74; N, 9.62. TLC (SiO2, toluene/ethyl acetate = 95/5 v/v): R_f = 0.37, 0.50, 0.67.

Synthesis of 1,3,5-Tris(2-cyano-2-ethoxycarbonylethenyl)-benzene (CVB-S3). TFB (3.24 g, 20 mmol), ethyl cyanoacetate (13.56 g, 90 mmol), acetoamide (0.5 g), toluene (50 mL), and acetic acid (20 mL) were allowed to react at 104 °C for 9 h. The residue was extracted with toluene (100 mL) and washed with water. The toluene solution was dried over magnesium sulfate. The toluene was evaporated under a reduced pressure to give the crude product (12.6 g), which was recrystallized from a hexane/benzene (1/1 v/v) solution. A total of 2.6 g of crystalline powder was obtained (29 % yield). Mp: 134 °C. IR (KBr, cm^{-1}): 3060 (m, Ph), 3050 (m, Ph), 3000 (m, Ph), 2950 (m), 2910 (m), 2230 (s, CN), 1740, 1720 (vs, C═O), 1605 (vs, ph), 1260 (vs, C−O). H-NMR ($CDCl_3$, ppm): 8.30 (s, CH═, 1 H), 8.04 (s, Ph−H, 1 H), 4.20 (q, OCH_2−, 2 H), 1.20 (t, $-CH_3$, 3 H). Anal. calcd. for $C_{24}H_{21}N_3O_6$: C, 64.42; H, 4.73; N, 9.39. Found: C, 67.25; H, 4.93; N, 8.52. TLC (SiO_2, toluene/ethyl acetate = 95/5 v/v): R_f = 0.23 (broad).

Synthesis of 1,3,5-Tris(4-t-butylphenyl-1,3,4-oxadiazoyl)-benzene (OXD-S1). Commercial 1,3,5-benzene ticarbonyl trichloride (2.0 g, 7.5 mmol, Aldrich) was refluxed in 20 mL of phosphorous oxychloride for 3 h. The phosphorous oxychloride was removed and dried under a reduced pressure. 4-*tert*-Butylbenzoylhydrazide (8.0 g, Lancaster) and dry pyridine (30 mL) were added to the residue. The mixture was allowed to react at room temperature for 2 h and then at 80 °C for 2 h. The mixture was cooled and then poured into 500 mL of water to produce a precipitate. The precipitate was filtered and washed with dilute hydrochloric acid and with water. The precipitate was recrystallized from a methanol/ethanol mixed solution to give 1.7 g of needle crystals. Then, 1.0 g of the crystals and 30 ml of phosphorous oxychloride were refluxed for 5 h. The phosphorous oxychloride was removed under a reduced pressure. The residue was washed with water and recrystallized from an ethanol/toluene solution to give 0.66 g of white crystalline powders (22 % yield). Mp: 268 °C. IR (KBr, cm^{-1}): 2963 (s, *tert*-butyl), 1615 (s, Ph), 1495 (vs, −C═N−). H-NMR ($CDCl_3$, ppm): 9.05 (s, center Ph−H, 1 H); 8.15 (d, Ph−H, 2 H); 7.61 (d, Ph−H, 2 H), 1.40 (s, $-CH_3$, 9 H). Anal. calcd. for $C_{42}H_{42}N_6O_3$: C, 74.3; H, 6.2; N, 12.4. Found: C, 74.8; H, 6.1; N, 12.4.

Measurement of Thermal Properties. The thermal properties were determined by differential scanning calorimetry (DSC) using a Mettler FP-900 thermal analyzer. Polycrystalline samples of 2−5 mg were put in aluminum pans and heated at a scan rate of 10°/min. The phase transition temperatures (T_{tr}) and the corresponding enthalpy changes were measured. Indium metal was used as the standard. After they were melted, the samples were cooled at the same rate to observe the crystallization temperature(T_{c2}). The compounds which underwent

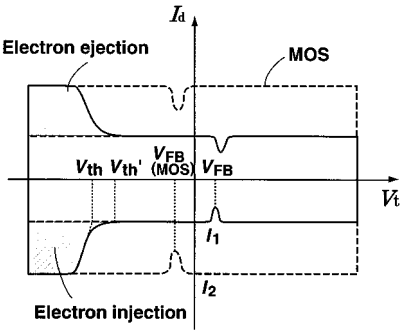

Figure 2. Schematic diagram of displacement current measurement.

crystallization were quenched to form glasses by inserting them in their fused states into liquid nitrogen or by putting them on a cooled aluminum block. The resulting glasses were heated again under the same conditions to measure the glass transition temperature (T_g) and crystallization temperature (T_{c1}). The thermal properties of all the amorphous compounds except the CVB compounds and TCPE have been outlined in previous papers.[4,5]

Measurement of Optical Properties. Absorption spectra of dilute solutions in nonpolar solvents and amorphous films formed on glass sheets were measured with a Shimadzu UV-260 spectrophotometer.

Film Formation. Thin films were produced with a conventional physical vapor deposition system of our own making with a molecular turbopump. The typical conditions were as follows: pressure, 3×10^{-4} Pa; substrate temperature, room temperature, not cooled; source, tungsten heating vessel; deposition speed, 0.1−0.5 nm/s; distance of the evaporation source and a substrate, about 20 cm. The film thickness was controlled to be 40−200 nm using a quartz balance.

Measurement of Electrical Properties. Electric carrier injection from electrodes to organic thin films and ejection of injected carriers from organic films to electrodes were observed at the atmospheric pressure or in a vacuum using a displacement current technique developed by us.[6]

The displacement current characteristics were measured for a structure of metal/organic/SiO_2/Si (M/Org/OS). Capacitance−voltage measurements of metal/SiO_2/Si (MOS) capacitors at low-frequency thermal equilibrium conditions have been applied to determine the surface-state densities of the oxide layer. The currents (I_d) of MOS devices were expressed by the capacitance (C_t) and a periodically applied ramp bias (V_t),

$$I_d = C_t dV_t/dt$$

As a result, the voltage independent currents were observable at the accumulation and inversion biases, while sharp dips relevant to the flat-band voltage [V_{FB}(MOS)] appeared at the depletion region (broken curve described as MOS in Figure 2). The M/Org/OS has a single M/Org interface, and the organic layer is brought into contact with the SiO_2 insulator. In the simplest case where the organic layer behaves as only a dielectric, the voltage independent currents can also be observed, corresponding to the geometric capacitance. However, for most M/Org/OS devices consisting of donor or acceptor molecules, the carrier injection or ejection through the M/Org interfaces prevails, when applying a cyclic voltage ramp at a frequency maintaining a quasistatic condition. The charged carriers pass through into the organic layer and accumulate mostly at the Org/SiO_2 interfaces. The observed displacement currents [I_d-(V_t)] are hence voltage dependent and will be sensitive to the changes in the carrier densities concerned.

Organic thin films of about 30−50 nm thick were prepared by physical vapor deposition onto a thermally oxidized SiO_2 of n-type (impurity concentration ion of 5×10^{14}/cm^3). The 1 mm diameter metal electrode of Al or Au was then evaporated using pattered shadow mask, yielding the structure of M/Org/OS.

A 0.01 Hz triangle bias (±10 V) was repeatedly applied to the devices with irradiation of infrared light to generate carriers in the Si plates. The displacement current was increased by the injection and transport of electric carriers. The principle of displacement current diagram is shown schematically as a solid curve in Figure 2. The apparent ionization potential (I_p) or electron affinity (E_A) values can be described by the following equation assuming that the thermodynamic injection and ejection of carriers take place:

$$E_A \text{ or } I_p = W_m + (1 - I_1/I_2)(V_{th} - V_{FB})$$

where W_m denotes the work function of the electrode metal (M) and V_{FB} is regarded as the effective zero-field bias of the device. $(1 - I_1/I_2)(V_{th} - V_{FB})$ equals $[C_{SiO2}/(C_{Org} + C_{SiO2})](V_{th} - V_{FB})$, which presents the net voltage applied to the organic film. V_{FB} sometimes shifts from the MOS position [V_{FB}(MOS)]due to the charges accumulated in the organic film. V_{th}' in Figure 2 indicates the start of current increase. Impurity carriers often give an unclear V_{th}', and cause V_{th}' to differ significantly from V_{th}.

Quantum Chemical Calculations. A Pariser−Parr−Pople (PPP) MO program was purchased from Maruzen and was used in a personal computer. The PPP calculation deals only with π-electrons. The results can be reliable because π-electrons almost determine the optical and electric properties of dyes in this paper. Large molecules without exact nuclear coordinates can be calculated. Calculation time is short even using a personal computer. This is suitable for determining calculation parameters by trial and error. The PPP method is one of the semiempirical methods. Determining calculation parameters is the most important to get reliable and quantitative results.

Optical and electric properties are those in a condensed matter, that is, in an amorphous state, not in a vacuum. However, quantum calculations, in principle, deal with molecules in a vacuum. In a condensed matter, ionic species can be stabilized by polarization energies (P). The polarization energies are generated by reorientation of atoms or molecules and by localization of electric charges. Therefore, observed ionization potential values (I_p) decrease, and observed electron affinity values (E_A) increase in a condensed matter. In the calculation, this corresponds to that HOMO and LUMO energy levels substantially shift to a shallower level and to a deeper level, respectively. Exited states obtained by light absorption have polar structures and are generally stabilized by the polarization energies. Therefore, how to estimate P is important in the PPP method.

In order to estimate the polarization energy (P), I_p parameters in the PPP program were modified so that the I_p parameters for donor heteroatoms were decreased and those for acceptor heteroatoms were increased. In the calculation, an I_p increment corresponds to an E_A increment.

The PPP method deals planar molecules in principle. However, many amorphous dyes shown in Figure 1 can be considered to take nonplanar structures. In order to estimate steric hindrance, we have considered resonant integrals (β) of particular bonds. Absolute values of β are the affinity energies between π-electrons and atom cores. The affinity energy for a weak conjugated bond is smaller than that for a strong conjugated bond. In the PPP method, β is calculated by the

TABLE 1: Thermal Properties of Electron Transport Dyes with Cyano Groups

compound	T_m[a] (K)	T_g[b] (K)	T_c[c] (K)	T_d[d] (K)
CVB-1	453	nc[e]	363	430
CVB-2	~410	330	no[g]	430
CVB-3	403	nc	318	400
CVB-4	473	na[f]		
CVB-S1	543	nc	346	530
CVB-S2	~540	319	no	510
CVB-S3[h]	407	286	no	430
TCPE[i]	505	330	384	480

[a] Melting point. [b] Glass transition temperature. [c] Crystallization temperature. [d] Vacuum deposition temperature. [e] nc = not clear. [f] na = no amorphous state was formed. [g] no = not observed. [h] Crystal transition was observed (T_{tr} = 348 K). [i] Polymorphisms were observed (T_m = 481 K).

following equation (variable β method[10]):

$$\beta = A_0 + A_1 B$$

where A_0 and A_1 are parameters with negative values, and B is a bond order. B is changed every self-consistent field (SCF) calculation cycle. We increased A_0 values for weak conjugated bonds due to steric hindrance.

These parameters were modified so that the calculated absorption wavelengths (λ(calcd)) agreed with the observed absorption wavelengths (λ(obsd)) for the solution samples.

Results and Discussion

Thermal Properties. Table 1 lists the thermal properties of CVB compounds and TCPE. The thermal properties of other dyes have already been reported in previous papers.[4,5] The melting points of 1,3,5-tris(substituted) compounds (CVB-S1 and CVB-S2) with a large molecular weight were higher than those of 1,3-bis(substituted) compounds (CVB-1 and CVB-2). The DSC melting peaks were broad for cyanophenyl compounds (CVB-S2 and CVB-2). The melting point of 1,3,5-tris(2-cyano-2-ethoxycarbonyl)benzene (CVB-S3) was lower than the melting points of the other 1,3,5-tris(substituted) compounds and was similar to that of 1,3-bis(2-cyano-2-ethoxycarbonyl)benzene (CVB-3). Glass transition temperatures (T_g) for the tris-(substituted) compounds were similar to those of the bis-(substituted) compounds. More cis−trans configurations at the three vinyl linkages for the tris(substituted) compounds probably decrease T_g values in spite of large molecular weights.

CVB-S1, -S3, and OXD-S1 gave the single spot in the TLC. In the case of CVB-S3, although it is the mixture of cis and trans compounds, both CN and C=O substituents are electron-withdrawing groups. Therefore, a large difference is not given in each isomer. On the other hand, CVB-S2 possesses both electron-donating and large phenyl groups and electron-withdrawing CN groups. The CVB-S2 isomers of cis and trans gave three spots in the TLC chart, a complex NMR spectrum, and a broad melting peak.

The amorphous states of the tris(substituted) compounds were more stable than those of the bis(substituted) compounds. No crystallization was observed for CVB-S2 and CVB-S3 in the DSC measurement. The linear *p*-bis(substituted) compound (CVB-4) did not form an amorphous state. TCPE formed an amorphous state with a T_g of 330 K, and this amorphous state changed to a crystalline state at 384 K.

Film Forming Properties. Table 1 lists deposition vessel temperatures (T_d) at which the deposition rates reached 0.1−0.5 nm/s. T_d can been seen to roughly correspond to the melting points (T_m). This means that vaporization of the compounds takes place near T_m. Polarized optical microscope observation indicated that small crystals were observed in CVB-1, CVB-3, and CVB-4 films just after deposition. CVB-2 and CVB-S compounds produced uniform amorphous thin films. Uniform amorphous films of TCPE turned to crystalline films after they were allowed to stand for 2 days at room temperature.

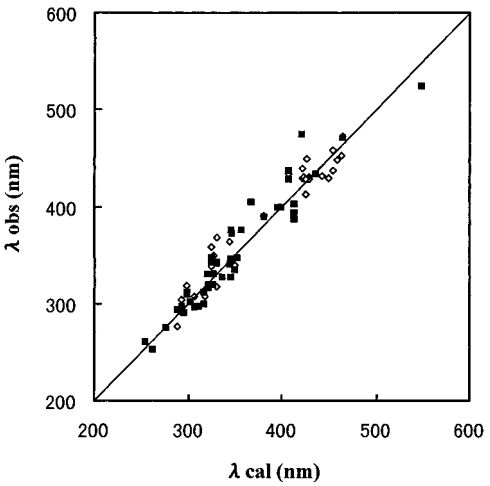

Figure 3. Correlation between observed absorption wavelength (λ_{obs}) and calculated wavelength (λ_{cal}): (■), solution, (◇), amorphous film.

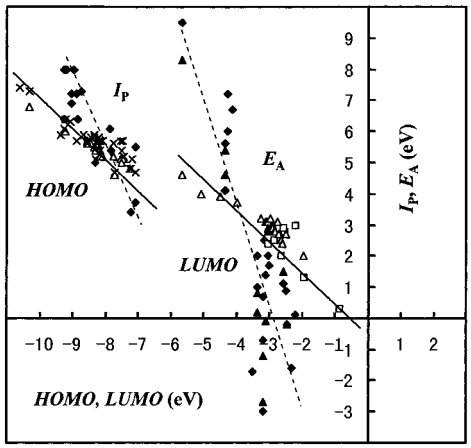

Figure 4. Correlation between observed ionization potential (I_P) and electron affinity (E_A) values and calculated HOMO and LUMO energy levels: (♦), DC in a vacuum; (▲), DC in air; (×), PE; (△), CV; (□), PC. See the footnotes of Tables 2 and 3.

Light Absorption Properties. Table 2 lists the observed light absorption wavelengths (λ_{obs}) and their calculated values (λ_{cal}) for various dyes. The calculation parameters of several heteroatoms in the PPP program were determined as summarized in the footnotes of Table 2. The initial values were also shown.

Using these new parameters, the calculated λ_{cal} values were found to correspond to λ_{obs} as shown in Figure 3. Figure 3 also indicates that the λ_{obs} values for amorphous films are nearly equal to those for solution samples. This suggests that the polarization energies in amorphous states are similar to those in nonpolar solvents.

Carrier Injection Properties. Tables 2 and 3 list the electrical properties of dyes. Figure 4 shows the correlation between the observed ionization potential (I_p) and electron affinity (E_A) values and the calculated HOMO and LUMO energy levels.

The solid straight lines with a slope of −1 in the figure indicate that the HOMO and LUMO energy levels calculated by the PPP method correspond with real I_p and E_A values, respectively, measured by the photoelectron emission (PE), photocurrent (PC), and cyclic voltammetry (CV) methods.

TABLE 2: Optical and Electrical Properties of Various Dyes

		λ_{obs}				E_A				I_P					λ_{obs}					E_A				I_P			
compound	λ_{cal}[a] (nm)	film (nm)	sol[b] (nm)	ref	LUMO (eV)	PC[c] (eV)	CV[d] (eV)	ref.	HOMO (eV)	DC[e] (eV)	PE[f] (eV)	CV (eV)	ref	compound	λ_{cal}[a] (nm)	film (nm)	sol[b] (nm)	ref	LUMO (eV)	PC[c] (eV)	CV[d] (eV)	ref.	HOMO (eV)	DC[e] (eV)	PE[f] (eV)	CV (eV)	ref
TCNQ	413		394 D	tw[h]	−5.65		4.6	20	−10.6		7.4		23	BSA-17	454	458		16	−2.76		3.1	16	−7.44		5.2	5.1	16
C60							4.2	21						BSA-16	454	437		16	−2.7		2.7	16	−7.46		5.7	5.1	16
BQ	435		434 C	15	−5.06		4	20	−11.8					OXD-S8	327	350	331 D	tw	−2.62				−9.02	7.2			
NQ	413		403 Et	15	−4.5		3.9	20	−10.8					anthracene	356		376 C	tw, 17	−2.62	2	2.5	20, 23	−8.57		5.7	5.6	20, 23
CVB-S1	306		298 D	tw	−4.36				−11.31					pyrene	346		373 C	17	−2.61		2.4	21, 23	−8.58		5.6	5.7	20
PO	441				−4.26				−9.35					BSA-1	449	429		16	−2.57				7.51		5.4	5	16
DPNTCI	549		525 D	tw	−4.14				−9					Alq3	380	391	390 D	tw	−2.56	2.9		24	−8.88	7.2	5.7		24
CVB-1	316		300 D	tw	−4.07				−10.91					DSB	345		376 D	18	−2.51	2.8		18	−8.68		5.9		18
AQ	367		405 Cl	tw, 15	−3.98		3.7	20	−10.5					BBOT	345		327 C	tw, 17	−2.5				−8.84	6.4			
TBAQ[g]	407	434	428 D	tw	−3.75				−9.22					BSA-2	463	453		16	−2.49		2.7	16	−7.27		4.8	4.8	16
DCDPBAQ[g]	413		387 D	tw	−3.5				−8.96					OXD-S3	298		312 D	tw	−2.46				−9.25	6.4			
CVB-4	345		346 D	tw	−3.38				−9.76					PPCP	344	364	341 C	tw	−2.43				−8.76	7.3			
BSA-7	428	431		14	−3.25		3.2	16	−8.46		5.8	5.6	16	PBBO	336		327 D	tw	−2.41				−8.95	8			
CVB-S2	321		320 D	tw	−3.2				−9.78					OXD-S1	293	304	297 D	tw	−2.3				−9.24	8			
TCPE	326		320 D	tw	−3.17				−9.67					OXD-B1	302		302 D	tw	−2.2	3		24	−9.06		6.3		24
DNIBPC	325	339	343 D	tw	−3.16				−9.6					OXD-S6	298	319	310 D	tw	−2.2				−9.05	6.9			
CVB-2	321		316 D	tw	−3.11				−9.68					OXD-7	292	294	292 D	tw, 19	−2.19				−9.19	8			
DCM	464	473	471 E	tw	−3.11				−8.11					PQP	288	276	294 C	17	−2.09				−9.1				
BSA-14	425	413		16	−3.1		3.1	16	−8.35		5.9	5.5	16	naphthalene	317		312 C	17	−1.96	1.3	2	20, 23	−9.23		6.4	6	20, 23
BSA-15	426	428		16	−3.09		3.1	16	−8.33		5.8	5.5	16	p-terphenyl	275		275 C	17	−1.93				−9.26		6.1		25
BSA-13	428	428		16	−3.05		3.1	16	−8.27		5.6	5.4	16	OXD-S2	325	358	347 D	tw	−1.85				−7.9				
OXD-S5	306	308	297 D	tw	−3.04				−9.71					OXD-8	330	368	342 D	tw, 19	−1.84				−7.87	6.1			
CVB-3	311		297 D	tw	−3.03				−9.9					ASPP	395		400 D	tw	−1.81				−7.07	3.7	4.7		26
tetracene	420		475 B	17	−3.02	2.4	2.9	22	−8.17		5.4	5.4	20, 23	DEPB	399		400 D	tw	−1.77				−7.22	3.4	4.8		26
CVB-S3	306		296 D	tw	−3.01				−9.93					TPHB	262		253 C	tw, 17	−1.74				−9.45				
BSA-8	426	449		16	−2.98		3.2	16	−8.2		5.7	5.7	16	CZ	295		291 C	17	−1.68				−9.36		5.9		20
BSA-5	422	439		16	−2.95		2.9	16	−8.24		5.6	5.4	16	C2	350	340	335 D	tw	−1.31				−7.44				
BSA-11	442	432		16	−2.94		3	16	−7.78		5.6	5.2	16	OXD-M1	352		347 C	tw	−1.09				−7.19		5.1		26
BSA-6	422	429		16	−2.9		2.9	16	−8.19		5.8	5.4	16	benzene	254		261 C	17	−0.85	0.3		20	−10.3		7.3	6.8	20
BSA-12	458	448		16	−2.9		3	16	−7.53		5.7	5.1	16	DIAMINE	318	308		tw	−0.38				−7.85	5.4			
BSA-4	423	431		16	−2.88		2.9	16	−8.16		5.7	5.2	16	TMPD	320		331 C	17	−0.36				−7.74		4.7	4.6	20
perylene	407		437 C	17	−2.87	2.5	2.8	20, 23	−8.32	5	5.1	5.4	20, 23	TPB	330	318	343 C	tw	0.63				−7.09	5.4			
BSA-3	425	428		16	−2.81		2.8	16	−8.08		5.7	5.2	16														

[a] I_P(N in CN) = 19.0 eV (initial value: 14.18 eV); $\boldsymbol{A}_0$(NC) = −5.0 eV (−2.675 eV); I_P(O in BQ, NQ, AQ) = 20.8 eV (17.7); $\boldsymbol{A}_0$(C═N in OXD) = −2.3 eV(−2.0); $\boldsymbol{A}_0$(N−N in OXD) = −2.0 eV; I_P(N in OXD) = 14.12 eV (14.12); I_P(hydrogen-bonding N in OXD) = 16.0 eV; $\boldsymbol{A}_0$(Ph−Ph) = −1.8 eV(−2.04); $\boldsymbol{A}_0$(═C−Ph in BSA) = −1.50 eV(−2.04); I_P(N in Ph3N) = 24.0 eV(26.7); I_P(N in Alq3) = 16.0 eV(14.12); I_P(O^- in Alq3) = 29.0 eV(26.70); I_P(N in MPT ethyl carbazol) = 26.7 eV (26.7); I_P(N in TMPD) = 26.5 eV (26.7); I_P (N in CZ) = 32.0 eV (26.7); $\boldsymbol{A}_0$(Ph−Ph) = −1.8 eV(−2.04); $\boldsymbol{A}_0$(═C−(Ph)2) = −1.4 eV (−2.04). [b] B, benzene; C, cyclohexane; Cl, chloroform; D, 1,4-dioxane; E, ethanol; Et, diethyl ether. [c] E_g(band gap) was measured by photoconduction. $\boldsymbol{E}_A = I_p(PE) - \boldsymbol{E}_g$. [d] Cyclic voltammetry $I_P = \boldsymbol{E}_{ox}$(vs SCE) + 4.5. [e] Displacement current was measured in vacuum. [f] Photoemission was measured with ACl or by ultraviolet photoelectron spectroscopy. [g] Calculated as a ═CH2 terminated half instead of a whole molecule. [h] tw = this work.

TABLE 3: Electron Injection and Ejection Properties of Various Dyes

compound	state[a]	electrode	condition[b]	LUMO (eV)	E_A[c] (eV) vacuum	E_A[c] (eV) air	reversibility[d]	ca[e]	note[f]
TCNQ	cryst	Al	vac	−5.65					ct
TCNQ	cryst	Au	vac	−5.65	9.5		very good	no	ic
TCNQ	cryst	Au	air	−5.65		8.3	very good	no	ic
C60		Al	vac		7.8		fair	no	ct
CVB-S1	amor	Al	vac	−4.36	4.1		good	no	ic
CVB-S1	amor	Al	air	−4.36		4.6	bad	no	ic
CVB-S1	amor	Au	vac	−4.36	5.6		good	no	ic
CVB-S1	amor	Au	air	−4.36		5.4	bad	no	ic
PO	amor	Al	vac	−4.26	6		very good	no	ic
PO	amor	Au	vac	−4.26	7.2		very good	no	ic
DPNTCI	cryst	Al	vac	−4.14	6.7		very good	no	
DPNTCI	cryst	Al	air	−4.14		nc		no	ic
CVB-1	cryst	Al	vac	−4.07	nc			no	ic
CVB-1	cryst	Al	air	−4.07		nc		no	ic
DCDPBAQ	amor	Al	vac	−3.5	−1.7		fair	yes	
CVB-4	cryst	Cu	vac	−3.38	1		very good	no	
CVB-4	cryst	Cu	air	−3.38		0.2	good	no	
CVB-4	cryst	Al	vac	−3.38	2		very good	no	
CVB-4	cryst	Al	air	−3.38		0.8	good	no	
CVB-S2	amor	Al	vac	−3.2	−3		very good	yes	
CVB-S2	amor	Al	air	−3.2		−2.7	very good	yes	
TCPE	amor	Al	vac	−3.17	−0.7		very good	nc	
TCPE	amor	Al	air	−3.17		−1.2	very good	nc	
TCPE	cryst	Al	vac	−3.17	0.7		good	no	
TCPE	cryst	Al	air	−3.17		nc			ic
DNIBPC	amor	Al	vac	−3.16	2.5		very good	no	
CVB-2	amor	Al	vac	−3.11	1.4		bad	no	
CVB-2	amor	Al	air	−3.11		−0.1	bad	no	
OXD-S5	amor	Al	vac	−3.04	2.8		bad	no	
OXD-S5	amor	Al	air	−3.04		2.8	bad	no	
CVB-3	cryst	Al	vac	−3.03	2		fair	no	
CVB-3	cryst	Al	air	−3.03		nc	bad	no	ic
CVB-S3	amor	Al	vac	−3.01	1.7		fair	no	
Alq3	amor	Al	vac	−2.56	1.1		very good	little	
Alq3	amor	Al	air	−2.56		1.5	very good	little	
BBOT	amor	Al	vac	−2.5	0.9		very good	no	
OXD-S3	amor	Al	vac	−2.46	−0.2		good	little	
OXD-S3	amor	Al	air	−2.46		−0.2	good	little	
OXD-S1	amor	Al	vac	−2.3	−1.6		very good	yes	
OXD-7	amor	Al	vac	−2.19	0.1		very good	yes	
OXD-7	amor	Al	air	−2.19		−2	fair	yes	
ASPP	amor	Al	vac	−1.81					ni
DIAMINE	amor	Al	vac	−0.38					ni

[a] amor = amorphous state, cryst = crystalline state. [b] Measurement condition; vac = vacuum; cycle frequency = 0.01 Hz. [c] Calculated from V_{th} in Figure 2. [d] Reversibility of displacement current feature. [e] Charge accumulation in the film. nc = not clear. [f] ct = charge transfer with the electrode was observed. ic = impurity carrier was observed. ni = no injection.

Therefore, the I_p and E_A values in the condensed states can be estimated by the PPP method tuned to reproduce the experimental absorption wavelengths (λ_{obs}). This indicates that the polarization energies (P) in the condensed states are correctly estimated by the modified PPP parameters. The effects of substituent groups can also be predicted by the PPP method. The measurement samples, except for those for CV, were thin films in the amorphous or crystalline states, depending on the molecules shown in Table 3.

The properties of electric carrier injection from metal electrodes to dye films can be described by the *apparent* I_p and E_A values. Small apparent I_p values indicate that positive holes can be easily injected into the films from the electrodes. Large apparent E_A values indicate that injection of negative electrons from the electrodes into the films is easy. The dashed lines also indicate that a rough correlation between the HOMO and LUMO levels and the injection properties have been established. However, the data scatter was large. The nonequilibration of the displacement current is thought to be one of the reasons for the scatter. For many dyes, measurement at 0.01 Hz is not sufficiently slow for thermodynamic equilibrium to be reached.

Electrical carriers were more readily injected into strong donor and acceptor molecules than predicted from the real I_p and E_A values. Conversely, injections into weak donor and acceptor molecules were more difficult than expected. In the latter case, the difficulty was often caused by carriers accumulated in the film (V_{FB} shift).

The carrier injection properties can be considered to be affected by various factors. The I_p and E_A values of the molecules have large effects. One of the main causes of the deviation of the apparent I_p and E_A values from the real values is the presence of impurities in the atmosphere, including oxygen,[11] for p-type donor compounds and alkali metal ions and amines for n-type acceptor compounds. We found that organic thin films which were prepared and measured in a high vacuum without being exposed to the air showed the injection properties corresponding nearly to the real I_P and E_A values.[11]

Strong acceptors and donors carry out a charge-transfer reaction with the component in air, or an electrode, and tend to generate impurity carriers. Since this has good convenience to electric conduction and the trap of the carrier is hard to be carried out, V_{FB} shift is small. However, this is inconvenient for pushing up carriers to a high energy level in EL devices or solar cells.

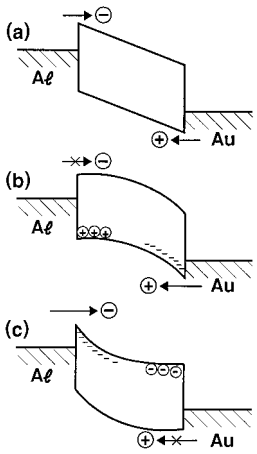

Figure 5. Schematic explanation of the effects of impurities on carrier injection properties: (a) intrinsic state without impurities, (b) p-type film, and (c) n-type film. The dashes (− −) indicate impurity states.

Other effects such as molecular orbital localization, trapping sites by local dipoles,[12] and interfacial interaction between the electrode and the molecules[13] are expected to be present. A schematic explanation is presented in Figure 5. For intrinsic states, an electric field is applied uniformly to the organic film. In the case of an n-type film with negative carriers, a depletion layer makes the injection of electrons easier and restricts the injection of positive holes. For a p-type film, the impurity effect is opposite to that of the n-type film.

Carrier injection phenomena without the influence of impurities were generally observed for moderate acceptor dye films with a LUMO level about in a range of about −2 to −4 eV.

Larger differences between the apparent E_A values in vacuum and under atmospheric pressure were seen for amorphous acceptor molecules with bend structures such as CVB-2 and OXD-7 than for acceptor molecules with symmetric and globular structures, such as CVB-S1, CVB-S2, TCPE, OXD-S2, OXD-S1, and Alq3. The bend amorphous dyes possess a large dipole moment due to their unsymmetrical structures. However, due to their symmetrical structures, the globular compounds did not have a large dipole moment. These results suggest that the impurity carriers are easily generated by the interaction between the bend molecules and the component in air. The resulting ionic or polar species can be considered to be stabilized by the dipoles.

Large differences between the apparent E_A values in vacuum and under atmospheric pressure were also seen for the polycrystalline films of TCNQ, CVB-4, CVB-3, DPNTCI, and TCPE. This is probably caused by impurity carriers that are trapped between heterogeneous polycrystalline structures.

Carrier injection and Ejection Reversibility. Figure 6 shows displacement current diagrams for some acceptor dyes with cyan groups and C_{60}. Electrons can be injected more easily in the case of stronger acceptors. Carrier injection and ejection reversibilities were, however, observed for moderate acceptors.

Table 3 also shows the electron injection and ejection reversibility for various dyes. Symmetrical and globular amorphous dyes such as CVB-S2, TCPE, OXD-S1, and Alq3 showed good reversibility regardless of the V_{FB} shift. Bend amorphous dyes such as CVB-1 and CVB-2, however, did not show good reversibility in spite of having LUMO levels that were similar to those of the globular molecules. Linear crystalline molecule such as CVB-4, PO, and TCNQ showed good reversibility.

As stated earlier, the bend amorphous dyes possess a large dipole moment due to their unsymmetrical structures. Injected

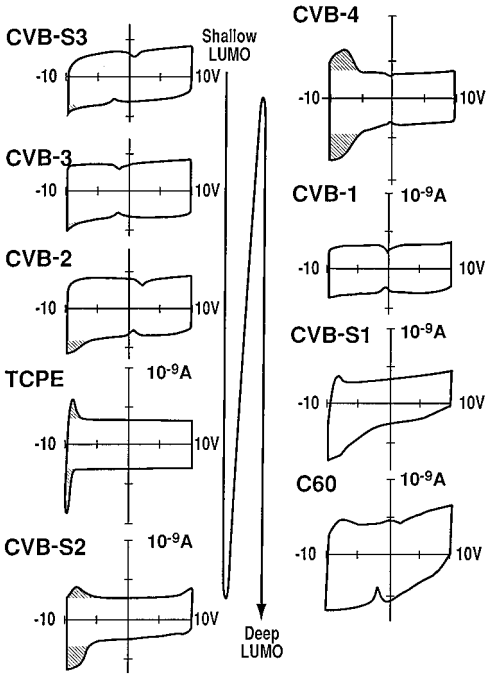

Figure 6. Displacement current diagrams for some acceptor dyes with cyano groups. Measurement condition: vacuum, 0.01 Hz, Al electrode.

electrons are easily trapped by the dipoles, and structural reorganization of the bend amorphous dye molecules probably takes place to stabilize the electrons. Amorphous structures with a free volume probably help this reorganization. In the globular amorphous dye films, a wide energy level distribution exists. Injected electrons are trapped in the deep levels, and the films are thus charged.[14] However, due to the low dipole moment, structural reorganization can be considered not to occur. In the case of crystalline films, also structural reorganization is thought to be unlikely.

Conclusion

Reversible electron injection and ejection properties without impurity effects could be obtained for the symmetric and globular amorphous molecules with an appropriate LUMO levels of about between −2 and −4 eV, which were calculated by the PPP method. New amorphous dyes with cyano substituents were found to be useful as electron transport materials.

Acknowledgment. We thank Ms. Y. Watanabe and Mr. M. Sasaki (Toshiba R&D Center) for performing displacement current measurement for some dyes. We also thank Dr. K. Ando, Mr. A. Miura, Mr. T. Nakayama, and Mr. S. Aoki (Toshiba R&D Center) for their helpful advice during the course of this study.

References and Notes

(1) (a) Tang, C. W.; VanSlyke, S. A. *Appl. Phys. Lett.* **1987**, *51*, 913. (b) Tang, C. W.; VanSlyke, S. A.; Chen, C. H. *J. Appl. Phys.* **1989**, *65*, 3610. (c) Adachi, C.; Tsutsui, T.; Saito, S. *Appl. Phys. Lett.* **1989**, *55*, 1489. (d) Adachi, C.; Tokito, S.; Tsutsui, T.; Saito, S., *Jpn. J. Appl. Phys., Part 1* **1988**, *27*, L713. (e) Greenham, N. C.; Moratti, S. C.; Bradley, D. D. C.; Friend, R. H.; Holmes, A. B. *Nature* **1993**, *365*, 628. (f) Egusa, S.; Gemma, N.; Miura, A.; Azuma, M. *IEICE Technical Report.* OME 90-40; Institute of Electronics, Information and Communication Engineers: Tokyo, 1990. (g) Hann, R. A. *Mol. Cryst. Liq. Cryst.* **1993**, *236*, 65.

(2) (a) Naito, K. *Appl. Phys. Lett.* **1995**, *67*, 211. (b) Naito, K. *Mol. Cryst. Liq. Cryst.* **1996**, *277*, 113.

(3) For example, see (a) Bondi, A. *Physical Properties of Molecular Crystals, Liquids, and Glasses*; John Wiley: New York, 1968; p 372. (b) Ngai, K. L., Wright, G. B., Eds. *Proceedings of the International Discussion*

Meeting on Relaxations in Complex Systems; *J. Non-Cryst. Solids*, **1990**, *131*−*133*. (c) Williams, G. *J. Non-Cryst. Solids*, **1990**, *123*, 75.

(4) Naito, K.; Miura, A. *J. Phys. Chem.* **1993**, *97*, 6240.

(5) Naito, K. *Chem. Mater.* **1994**, *6*, 2343.

(6) Egusa, S.; Gemma, N.; Miura, A.; Mizushima, K.; Azuma, M. *J. Appl. Phys.* **1992**, *71*, 2042.

(7) Bradley, D. D. C.; Bleyer, A.; O'Brien, D.; Weaver, M. S.; Lidzey, D. G.; Tajbakhsh, A.; Meng, S.; Fisher, T. A.; Pate, M. A.; Whittaker, D. M.; Skolnick, M. S. *Photoactive Organic Materials*; Kajzar et al., Eds.; Kluwer Academic Publishers: Netherlands, 1996; p 293.

(8) For example; see: (a) Rulliere, C.; Rayez, J. C.; Roberge, P. C. *Chem. Phys.* **1979**, *44*, 337. (b) Fabian, W. *Dyes Pigm.* **1985**, *6*, 341. (c) Frühbeis, H. *Melliand Textilber.* **1973**, *9*, 955. (d) Griffiths, J. *Rev. Prog. Color. Relat. Top.* **1981**, *11*, 37. (e) Griffiths, J. *Dyes Pigm.* **1982**, *3*, 211.

(9) Tokita, S.; Matsuoka, M.; Kogo, Y.; Kihara, H. *Molecular Design of Functional Dyes*; Maruzen: Tokyo, 1989; (In Japanese).

(10) Suzuki, H. *Electronic Absorption Spectra and Geometry of Organic Molecules*; Academic Press: New York, 1967; p 163.

(11) (a) Yamamoto, K.; Egusa, S.; Sugiuchi, M.; Miura, A. *Solid State Commun.* **1993**, *85*, 5. (b) Sasaki, T.; Egusa, S. *Jpn. J. Appl. Phys., Part 1* Submitted for publication.

(12) Hirao, A.; Nishizawa, H.; Sugiuchi, M.; *J. Appl. Phys., Part 1* **1993**, *74*, 1083.

(13) Imahigashi, T.; Hiramoto, M.; Yokoyama, M. *Prepr. of Annu. Meet. Chem. Soc. Jpn.* **1992**, *4A925*, 700.

(14) Naito, K.; Miura, A. *J. Am. Chem. Soc.* **1993**, *115*, 5185.

(15) Chemical Society of Japan, Ed. *Kagaku Binran Kisohen*; Maruzen: Tokyo, 1975; Vol. 2, p 1302, (*Handbook of Chemistry*, in Japanese).

(16) Sakon, Y.; Ohta, M. *IEICE Technical Report.* OME 92-17; Institute of Electronics, Information and Communication Engineers: Tokyo, 1992.

(17) Berlman, I. B. *Handbook of Fluorescence Spectra of Aromatic Molecules*; Academic Press: New York, 1971.

(18) Kusumoto, T.; Tokailin, H.; Higashi, H.; Hosokawa, C. *IEICE Technical Report.* OME 92-16; Institute of Electronics, Information and Communication Engineers: Tokyo, 1992.

(19) Hamada, Y.; Adachi, C.; Tsutsui, T.; Saito, S. *Jpn. J. Appl. Phys., Part 1* **1992**, *31*, 1812.

(20) Chen, E. C. M.; Wentworth, W. E. *Mol. Cryst. Liq. Cryst.* **1989**, *171*, 271.

(21) Allemand, P.-M.; Koch, A.; Wudl, F.; Rubin, Y.; Diederich, F.; Alvarez, M. M.; Anz, S. J.; Whetten, R. L. *J. Am. Chem. Soc.* **1991**, *113*, 1050.

(22) Torrance, J. B. *Mol. Cryst. Liq. Cryst.* **1985**, *126*, 55.

(23) Seki, K. *Mol. Cryst. Liq. Cryst.* **1989**, *171*, 255.

(24) Nakamura, H.; Kusumoto, T. *Prep. Annu. of Meet. Appl. Phys. Soc. Jpn.* **1993**, *29p-ZC-12*, 1126.

(25) Pope, M.; Swenberg, C. E. *Electronic Processes in Organic Crystals*; Clarendon: Oxford, 1982; pp 182−219.

(26) Mori, T.; Sugimura, E.; Mizutani, T. *IEICE Technical Report.* OME 89-51, Institute of Electronics, Information and Communication Engineers: Tokyo, 1989.